Materials Research Bulletin 46 (2011) 1755–1760

Contents lists available at ScienceDirect

Materials Research Bulletin

journal homepage: www.elsevier.com/locate/matresbu

Structural evolution of the double perovskites $Sr_2B'UO_6$ (B′ = Mn, Fe, Co, Ni, Zn) upon reduction: Magnetic behavior of the uranium cations

R.M. Pinacca [a,*], M.C. Viola [a], J.C. Pedregosa [a], R.E. Carbonio [b], M.J. Martínez Lope [c], J.A. Alonso [c]

[a] Área de Química General e Inorgánica "Dr. Gabino F. Puelles", Departamento de Química, Facultad de Química, Bioquímica y Farmacia, Universidad Nacional de San Luis, Chacabuco y Pedernera, 5700 San Luis, Argentina
[b] INFIQC (CONICET), Departamento de Fisicoquímica, Facultad de Ciencias Químicas, Universidad Nacional de Córdoba, Ciudad Universitaria, X5000HUA Córdoba, Argentina
[c] Instituto de Ciencia de Materiales de Madrid, C.S.I.C., Cantoblanco, 28049 Madrid, Spain

ARTICLE INFO

Article history:
Received 2 December 2010
Received in revised form 29 July 2011
Accepted 8 August 2011
Available online 17 August 2011

Keywords:
Perovskites
Uranium
Reduction
X-ray powder diffraction
Rietveld refinement
Magnetic behavior

ABSTRACT

We describe the preparation of five perovskite oxides obtained upon reduction of $Sr_2B'UO_6$ (B′ = Mn, Fe, Co, Ni, Zn) with H_2/N_2 (5%/95%) at 900 °C during 8 h, and their structural characterization by X-ray powder diffraction (XRPD). During the reduction process there is a partial segregation of the elemental metal when B′ = Co, Ni, Fe, and the corresponding B′O oxide when B′ = Mn, Zn. Whereas the parent, oxygen stoichiometric double perovskites $Sr_2B'UO_6$ are long-range ordered concerning B′ and U cations. The crystal structures of the reduced phases, $SrB'_{0.5-x}U_{0.5+x}O_3$ with $0.37 < x < 0.27$, correspond to simple, disordered perovskites; they are orthorhombic, space group Pnma (No. 62), with a full cationic disorder at the B site. Magnetic measurements performed on the phase with B′ = Zn, indicate uncompensated antiferromagnetic ordering of the U^{5+}/U^{4+} sublattice below 30 K.

1. Introduction

The so-called double perovskite $A_2B'B''O_6$ oxides contain two suitable B′ and B″ cations at the octahedral positions. Double perovskites may present different kind of cationic ordering at the octahedral sites as it has been reviewed by Anderson et al. [1]. The most common ordering is a rock-salt arrangement of the $B'O_6$ and $B''O_6$ octahedra in a perfectly alternated disposition along the three directions of the crystal. Double-perovskite oxides have attracted great interest in recent years, mainly due to their important physical properties, such as superconductivity [2,3], dielectricity [4,5] or magnetoresistivity [6–8].

The reduction of stoichiometric phases into novel oxygen hypo-stoichiometric oxides is a powerful tool for the development of new materials with novel magnetic or transport properties. Moreover, the stabilization of transition-metal perovskites with an adequate concentration of oxygen vacancies under reducing atmosphere can also be applied in new mixed electronic-ionic conductors for energy-conversion devices such as solid oxide fuel cells, oxygen separation membranes or solid oxide electrolyzers. For instance, Viola et al. [9] showed that the topotactic reduction of the stoichiometric Sr_2CoMoO_6 double perovskite leads to an oxygen hypo-stoichiometric perovskite $Sr_2CoMoO_{6-\delta}$ with ferromagnetic order above room-temperature and induced magnetoresistance. Furthermore, this oxide has also recently been proposed as anode material for SOFC evidencing a high performance even with wet CH_4 as a fuel [10].

Whereas the chemical reduction of $A_2B'B''O_6$ double perovskites with B″ = Mo, W has been investigated, this process has not been explored for uranium-containing $A_2B'UO_6$ phases. We have recently prepared and studied the structural and magnetic properties of oxygen-stoichiometric double perovskites $Sr_2B'UO_6$ with B′ = Mn, Fe, Co, Ni, Zn. The crystal structure is monoclinic (space group $P2_1/n$), as shown from XRPD data and NPD for the phase with B′ = Co. The B′–O distances obtained in the structural study suggest the presence of a partial disproportionation of the type $B'^{2+} + U^{6+} \Leftrightarrow B'^{3+} + U^{5+}$ for Fe, Mn and Ni cations [11,12].

As a natural continuation of our previous work, we found it interesting to investigate the conditions for the possible formation of reduced $Sr_2B'UO_6$ phases, by reduction with H_2/N_2 (5%/95%). We obtained and characterized disordered perovskites $SrB'_{0.5-x}U_{0.5+x}O_3$ with $0.37 < x < 0.27$. In this paper we report on the results of a XRPD study for these phases; the impact of the temperature control on the reduction process is analyzed. The optimum conditions for the synthesis of a well crystallized phase with a maximum amount of $SrB'_{0.5-x}U_{0.5+x}O_3$ perovskite were established; the macroscopic magnetic measurements for the phase with B′ = Zn with U^{5+}/U^{4+}

* Corresponding author. Fax: +54 2652430224.
E-mail address: rmp@unsl.edu.ar (R.M. Pinacca).

0025-5408/$ – see front matter © 2011 Elsevier Ltd. All rights reserved.
doi:10.1016/j.materresbull.2011.08.008

as unique and responsible of the magnetic behavior are presented and discussed.

2. Experimental

The $Sr_2B'UO_6$ double perovskites with B′ = Mn, Fe, Co, Ni, Zn were obtained as well-crystallized powders by the standard ceramic method [11]. Stoichiometric amounts of analytical grade $SrCO_3$, $B'CO_3$ and $UO_2(CH_3COO)_2$ were mixed, ground, placed in a platinum crucible and treated at 600 °C in air for 12 h and the resulting powder was reground and calcined at 900 °C for 12 h. Finally the product was fired at 1150 °C in air in four periods totaling 24 h with intermediate milling of the reaction mixture. For the $Sr_2B'UO_6$ phases with B = Mn and Fe the citrate-precursor method was used. The corresponding carbonates/acetates were dissolved in citric acid with formation of a resin which was decomposed at 700 °C in air. The precursor powders underwent a subsequent heating at 800 °C in air. Finally, the products were fired at 950 °C during 6 h in reducing atmosphere (1% H_2/99% Ar) in order to stabilize the Fe^{2+} and Mn^{2+} cations.

The initial identification and characterization of the final products was carried out by X-ray powder diffraction (XRPD) recorded at room temperature in a Rigaku D-MAX-IIIC diffractometer with Cu Kα (λ = 1.5406 Å) radiation. For the structural refinements the data were collected in 2θ steps of 0.02° and 5 s counting time in the range $10° \leq 2\theta \leq 120°$. The refinement of the crystal structures was performed by the Rietveld method [13] with the program Fullprof [14]. The peak profiles were modeled by a pseudo-Voigt function. The following parameters were refined in the final run: scale factors, background coefficients, zero-point error, pseudo-Voigt corrected for asymmetry parameters, positional coordinates, and isotropic thermal factors.

Thermal programmed reduction (TPR) curves were recorded in a Quanta Chrome Corp., model Chembet-3000 TPD/TPR device. The data were obtained between 25 and 1000 °C with a heating rate of 10 °C/min under a H_2/N_2 (5%/95%) flux of 20 mL/min.

The magnetic measurements were performed in a commercial superconducting quantum interference device magnetometer (SQUID) from Quantum Design. The magnetic susceptibility data were collected in the $4 < T < 400$ K range under an applied magnetic field of 0.1 T. Isothermal magnetization curves were obtained with magnetic fields up to 5 T at $T = 5$ K.

The FTIR spectra for Sr_2CoUO_6 and $SrCo_{0.5-x}U_{0.5+x}O_3$ with $x = 0.288(4)$ were recorded between 1000 and 350 cm^{-1} with a Nicolet-Magna 550 FTIR spectrometer, using the KBr pellet technique. In the investigated spectral range, the resolution was ±4 cm^{-1}.

3. Results and discussion

3.1. Sample preparation

These oxygen-stoichiometric $Sr_2B'UO_6$ perovskites (B′ = Fe, Mn, Co, Ni, Zn) were prepared as black (B′ = Fe, Mn, Co, Ni) or yellow (B′ = Zn) polycrystalline powders. In order to determine the optimum conditions for the preparation of well-crystallized reduced $Sr_2B'UO_6$ phases, a previous experiment was carried out with Sr_2CoUO_6. Fig. 1 shows the XRPD of the oxygen-stoichiometric phase at 25 °C and of the reduction products at different temperature. Fig. 2 displays the thermal programmed reduction (TPR) diagram of Sr_2CoUO_6. A wide band with center on 500–550 °C, a strong peak on 800–850 °C, and a weak peak at 400 °C that seems to be caused by impurities are observed. This indicates the existence of reduction processes above 500 °C for the main phase. Therefore, the oxygen-stoichiometric Sr_2CoUO_6 was treated by reduction in an H_2/N_2 (5%/95%) flow at 500, 550, 700, 800, 900 and 1000 °C for 10 h. Thermal treatments longer than 10 h did not produce changes in the obtained samples, suggesting that the reduction products reach equilibrium with the atmosphere after this treatment time.

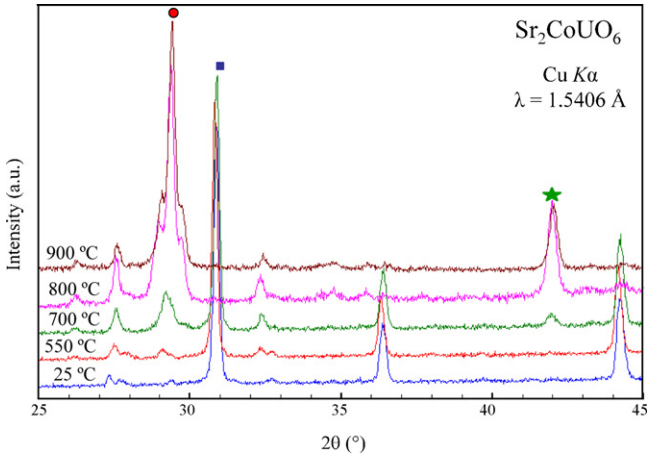

Fig. 1. XRPD for reduced Sr_2CoUO_6 taken at different temperatures of reduction with H_2/N_2 (5%/95%). The square represents the main reflection of ordered double perovskite $Sr_2B'UO_6$. The circle represents the main reflection of disordered simple perovskite $SrCo_{0.5+x}U_{0.5-x}O_3$. The star represents the main reflection of cobalt metal.

At 500 °C the reduction process did not occurs, but when the temperature is higher than 550 °C a new orthorhombic phase isostructural to $GdFeO_3$ [15] starts to appear (Fig. 1), with a chemical formula $SrCo_{0.5-x}U_{0.5+x}O_3$, as it will be described in the structural refinement Section 3.2. Upon the reduction process a Co^0 impurity appears (indicated with a star in the XRPD pattern); this fact is in agreement with the decrease of the Co content in the perovskite formula. There is a progressive decrease of the oxygen-stoichiometric Sr_2CoUO_6 double perovskite phase and an increment of the new disordered phase $SrB_{0.5-x}U_{0.5+x}O_3$, together with increasing amounts of elemental cobalt, as temperature rises. At 900 °C the quantity of the new perovskite phase is the biggest. The evolution of the initial stoichiometry Sr_2CoUO_6 along the solid solution $SrB_{0.5-x}U_{0.5+x}O_3$ with segregation of Co^0 implies the reduction of U^{6+} to U^{5+}/U^{4+}, since Co cannot adopt an oxidation state lower than 2+ within the perovskite structure.

The reduction of U^{6+} to U^{5+}/U^{4+} is also supported from infrared spectroscopy data: Fig. 3 shows the FTIR spectrum of the parent double perovskite and the reduced simple perovskite; the band assigned to the U–O antisymmetric stretching (ν_3) of the UO_6 octahedra of the reduced phase appears shifted to lower frequency

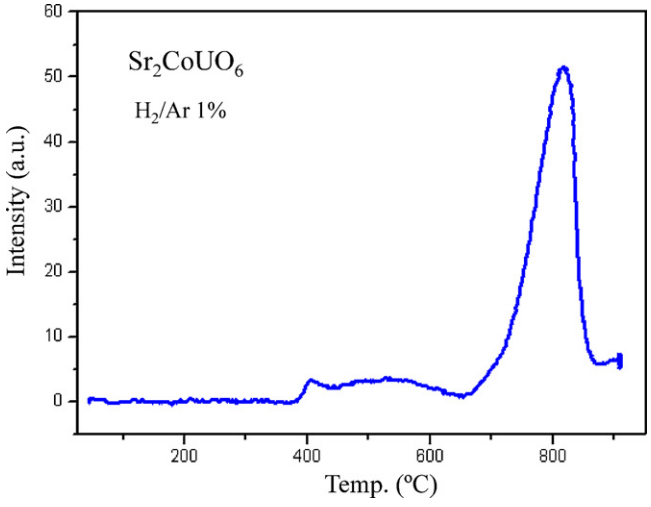

Fig. 2. TPR for double perovskite Sr_2CoUO_6.

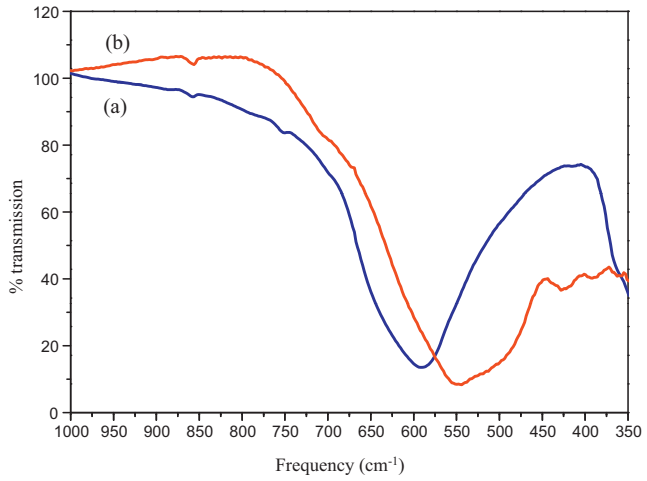

Fig. 3. FTIR spectra for samples Sr_2CoUO_6 (a) and $SrCo_{0.212(4)}U_{0.788(4)}O_3$ (b).

in comparison with the same group in the parent compound. In the original double perovskite the presence of the strongly polarizing U^{6+} cation implies strong U–O bonds with high vibration frequencies; the reduction of U^{6+} to U^{5+}/U^{4+} weakens the chemical bond and therefore the associated vibration frequencies decrease.

This preliminary study demonstrated that a reduced $Sr_2CoUO_{6-\delta}$ perovskite with oxygen vacancies is not obtained and, conversely, a new phase $SrB_{0.5-x}U_{0.5+x}O_3$ is stabilized with a maximum concentration at 900 °C. The structural study described below gives the details of the determination of the mentioned U-rich stoichiometry. In the same way the reduced phases $SrB'_{0.5-x}U_{0.5+x}O_3$ with B′ = Mn, Fe, Ni and Zn, were obtained as a dark polycrystalline powders in the same conditions as $SrCo_{0.5-x}U_{0.5+x}O_3$ at 900 °C.

3.2. Structural refinement

Fig. 4 displays a comparison of the XRPD patterns for all the reduced phases, showing the minor impurities present in each pattern. The crystallographic structures of $SrB'_{0.5-x}U_{0.5+x}O_3$ (B′ = Mn, Fe, Co, Ni, Zn) were refined from XRPD collected at RT in the orthorhombic Pnma space group (No. 62), Z = 4. Sr atoms were located at the 4c (*x*,1/4,*y*) positions, B′ and U distributed at

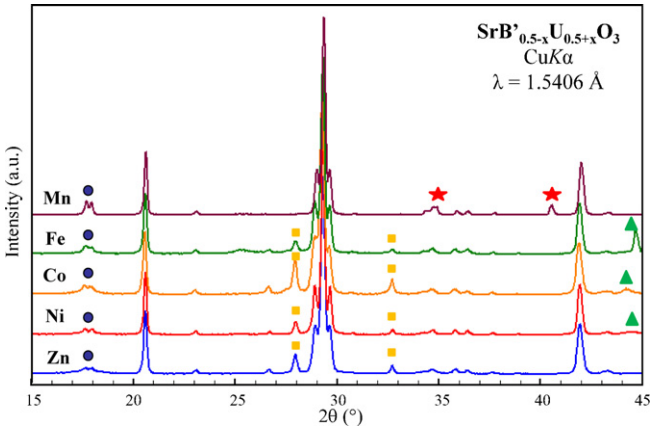

Fig. 4. XRPD pattern for the reduced materials recorded at room temperature. The oxygen-stoichiometric Sr_2CoUO_6 was treated by reduction in an H_2/N_2 (5%/95%) flow at 900 °C for 10 h. The circles correspond to the most intense impurity reflections Sr_3UO_6. Starts: MnO (B′ = Mn). Squares: $SrUO_{3.948}$. Triangles: metal element (B′ = Fe, Co, Ni).

Table 1
Unit cell parameters for $SrB'_{0.5-x}U_{0.5+x}O_3$ and reliability factors after the refinement from XRPD data at room temperature. Space group Pnma (No. 62).

	B′ = Mn	B′ = Fe	B′ = Co	B′ = Ni	B′ = Zn
a (Å)	6.1437(3)	6.1690(4)	6.1661(4)	6.1703(0)	6.1622(3)
b (Å)	8.5826(5)	8.6019(7)	8.6053(7)	8.6052(1)	8.5990(5)
c (Å)	6.0138(3)	6.0213(4)	6.0214(4)	6.0193(3)	6.0192(3)
V (Å^3)	317.11(3)	319.53(4)	319.50(4)	319.60(0)	318.78(3)
R_p (%)	8.59	13.20	10.40	10.40	9.97
R_{wp} (%)	10.90	15.80	13.30	13.30	12.40
R_{exp} (%)	8.29	10.00	8.90	8.49	8.53
χ^2	1.74	2.49	2.22	2.46	2.11
R_{Bragg} (%)	2.07	3.83	2.38	2.95	2.79

random at 2b (0, 0, 1/2) sites and oxygen atoms at the 4c (*x*, 1/4, *z*) and 8d (*x*, *y*, *z*) positions. $SrUO_{3.948}$, Sr_3UO_6 and metal B′ were included in the refinement as a second, third and fourth phases for B′ = Fe, Ni and Co, defined in the space groups R-3m, $P2_1/n$ and Fm-3m respectively. For B′ = Mn, Sr_3UO_6 and MnO are observed. Finally, for B′ = Zn, $SrUO_{3.948}$ and Sr_3UO_6 are included as second and third phases. We assume that ZnO is segregated as an amorphous phase to XRPD or disappears as vapor during the final heating. The Rietveld plots after the XRPD refinements are displayed in Fig. 5a–e, shows an excellent fit between observed and calculated profiles for these five compositions. The unit-cell parameters and the discrepancy factors after the refinements are listed in Table 1. Table 2 shows the most important structural parameters of the crystallographic structures for the five phases, $SrB'_{0.5-x}U_{0.5+x}O_3$ (B′ = Mn, Fe, Co, Ni, Zn). The most important bonding distances and angles are listed in Table 3.

Table 4 lists the value of *x* of the main perovskite phase. It is determined from the refinement of the mixed occupancy of B′ and U. Given the large difference between the scattering factors for B′ (belonging to the first transition series) and uranium, the value of *x* is determined with an excellent accuracy, with the standard deviation in the third decimal place. Table 4 also includes the

Table 2
Atomic parameters after the refinement from XRPD data for $SrB'_{0.5-x}U_{0.5+x}O_3$.

Atom	Site	*x*	*y*	*z*	Occ
B′ = Mn					
Sr	4c	−0.040(0)	0.25	0.026(1)	1
U	4b	0	0	0.5	0.822(4)
Mn	4b	0	0	0.5	0.166(4)
O1	4c	0.043(3)	0.25	0.605(3)	0.5
O2	8d	0.214(2)	0.063(2)	0.220(2)	1
B′ = Fe					
Sr	4c	−0.042(1)	0.25	0.021(1)	1
U	4b	0	0	0.5	0.872(6)
Fe	4b	0	0	0.5	0.128(6)
O1	4c	0.065(4)	0.25	0.636(4)	0.5
O2	8d	0.202(3)	0.070(2)	0.205(3)	1
B′ = Co					
Sr	4c	−0.043(1)	0.25	0.019(2)	1
U	4b	0	0	0.5	0.788(6)
Co	4b	0	0	0.5	0.212(6)
O1	4c	0.063(4)	0.25	0.619(4)	0.5
O2	8d	0.201(3)	0.068(2)	0.214(3)	1
B′ = Ni					
Sr	4c	−0.045(0)	0.25	0.017(1)	1
U	4b	0	0	0.5	0.792(2)
Ni	4b	0	0	0.5	0.216(2)
O1	4c	0.061(3)	0.25	0.623(3)	0.5
O2	8d	0.212(2)	0.068(2)	0.208(2)	1
B′ = Zn					
Sr	4c	−0.046(0)	0.25	0.015(1)	1
U	4b	0	0	0.5	0.774(4)
Zn	4b	0	0	0.5	0.232(4)
O1	4c	0.056(3)	0.25	0.622(3)	0.5
O2	8d	0.207(2)	0.068(2)	0.206(2)	1

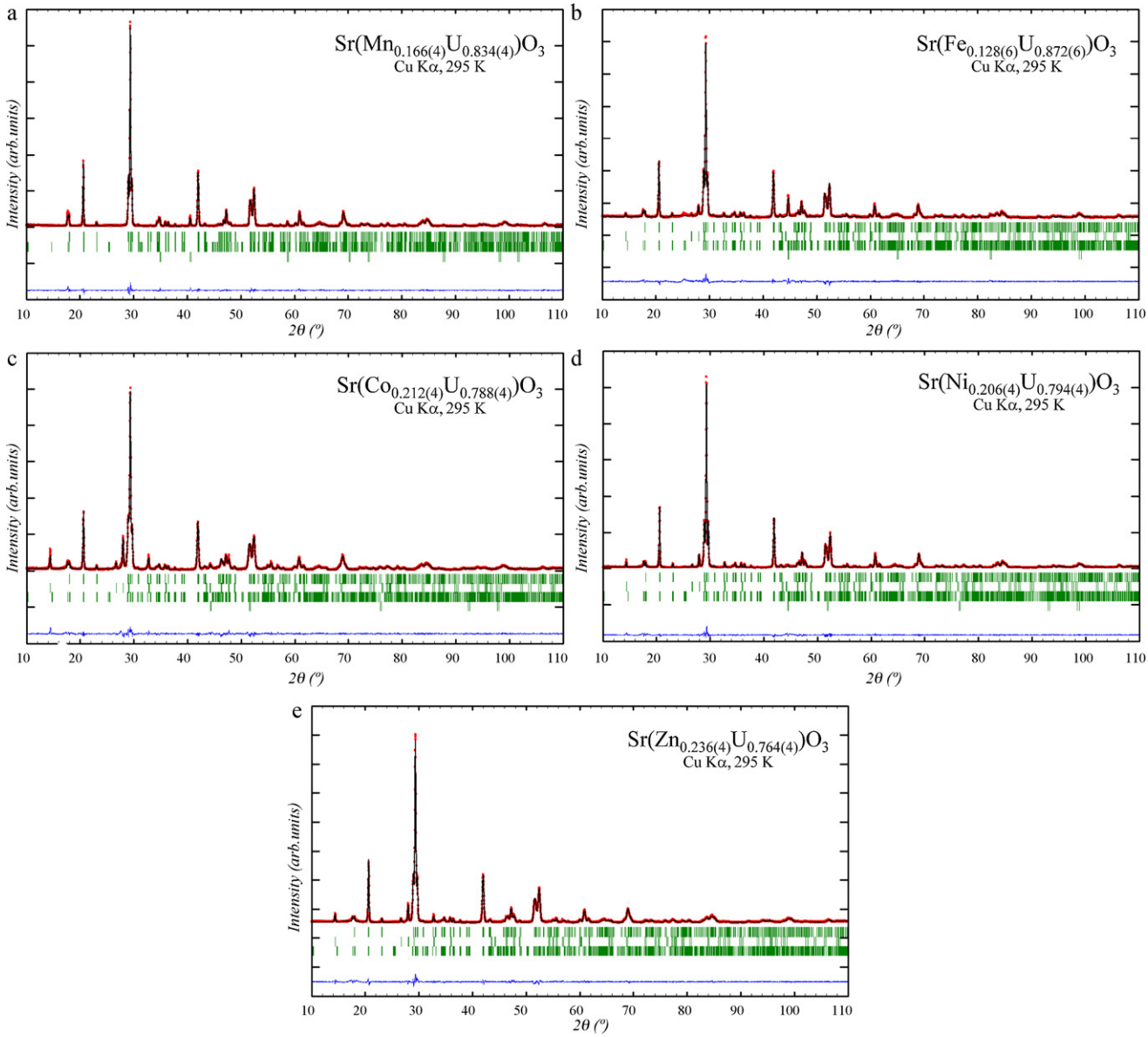

Fig. 5. Observed (dots), calculated (full line) and difference (bottom line) XRPD patterns after the refinement of the crystallographic structure of $SrB'_{0.5-x}U_{0.5+x}O_3$ at RT. The upper series of tick marks corresponds to the Bragg reflections of the main perovskite phase; the lower series correspond to the impurities as detailed in Table 4: (a) B′ = Mn, (b) B′ = Fe, (c) B′ = Co, (d) B′ = Ni, and (e) B′ = Zn.

nature and percentage of the different impurity phases present in each pattern.

The possibility that the main perovskite phases show a long-range ordering between the B′ and U cations over the octahedral sites of the perovskite was also checked in trial refinements in the monoclinic $P2_1/n$ space group, which contains two unequivalent sites for the B atoms. However, these trial refinements led to a worse agreement between the observed and calculated intensities of certain reflections or the refinement diverged. The reduced perovskite $Sr_2UO_{4.5}$ has been described in the Sr–U–O system under reducing conditions [16]; however trials to introduce $Sr_2UO_{4.5}$ as a second phase in the refinement of the different patterns were always unsuccessful.

The fact that the phase with B′ = Mn segregates MnO oxide instead of Mn metal upon reduction is in accordance with the high exothermic value of ΔG_f^o (MnO) = −362.90 kJ/mol, versus ΔG_f^o (FeO) = −254.40 kJ/mol, ΔG_f^o (CoO) = −214.20 kJ/mol and ΔG_f^o (NiO) = −211.70 kJ/mol. In the case of Zn, although we could not observe either ZnO or metal Zn, the low value of the Gibbs formation energy for ZnO, ΔG_f^o = −318.20 kJ/mol, leads us to believe that in this case ZnO is sublimated at the reaction temperatures. To check this hypothesis a blank experiment was totally clarifying: 0.5 g of ZnO powder placed in an alumina boat under a H_2/N_2 flow at 900 °C/12 h was completely lost by sublimation (and recrystallized in the cold region of the tubular furnace).

The two observed mechanisms of reduction upon segregation of either B′ or B′O are illustrated in Fig. 6.

4. Magnetic properties

As significant amounts of B′O or B′ metal were segregated for B′ = Mn, Fe, Co and Ni the magnetic properties for the corresponding reduced phases were not measured. For $SrZn_{0.236(4)}U_{0.764(4)}O_3$ the magnetic behavior only results from the electron injection on the uranium(VI) ion. From the refined stoichiometry the oxidation

Table 3
Main interatomic distances (Å) and angles (°) for $SrB'_{0.5-x}U_{0.5+x}O_3$ in the orthorhombic space group Pnma (No. 62) from the refinement. ϕ is the tilting angle of the (B′,U)O_6 octahedra.

	B′ = Mn	B′ = Fe	B′ = Co	B′ = Ni	B′ = Zn
SrO_8 (polyhedra)					
Sr_{4c}–O_{4c}	2.58(2)	2.41(2)	2.49(2)	2.46(2)	2.45(2)
Sr_{4c}–O_{4c}	2.68(2)	2.60(2)	2.56(2)	2.57(2)	2.59(2)
Sr_{4c}–O_{8d} *x*2	2.52(1)	2.43(2)	2.47(2)	2.73(1)	2.49(1)
Sr_{4c}–O_{8d} *x*2	2.68(1)	2.76(2)	2.75(2)	2.51(1)	2.76(1)
Sr_{4c}–O_{8d} *x*2	3.25(1)	3.23(2)	3.22(2)	3.22(1)	3.20(1)
<Sr–O_8>	**2.77**	**2.73**	**2.74**	**2.74**	**2.74**
B′,U–O_6 (octahedra)					
$(B',U)_{4b}O_{4c}$ (*x*2)	2.25(1)	2.34(1)	2.30(1)	2.31(1)	2.30(1)
$(B',U)_{4b}O_{8d}$ (*x*2)	2.21(1)	2.25(2)	2.20(2)	2.27(1)	2.26(1)
$(B',U)_{4b}O_{8d}$ (*x*2)	2.27(1)	2.30(2)	2.32(2)	2.25(1)	2.27(1)
<B′,U–O_6>	**2.24**	**2.30**	**2.28**	**2.27**	**2.27**
Angles around O					
(B′,U)–O_{4c}–(B′,U)	144.6(2)	134.0(3)	138.5(3)	137.8(2)	138.7(2)
(B′,U)–O_{8d}–(B′,U) (*x*2)	148.1(4)	142.9(6)	144.4(7)	145.2(4)	144.4(4)
<(B′,U)–O–(B′,U)>	**146.93**	**139.93**	**142.43**	**141.5**	**142.5**
ϕ	16.53	20.00	18.78	19.25	18.75

Distances longer than 3.3 Å have not been regarded. In bold: Average distances.

Table 4
Main phases and impurities obtained in each refinement.

Main phase (%, w/w)	Impurities (%, w/w)		
$SrMn_{0.166(4)}U_{0.834(4)}O_3$: 47.9(7)	Sr_3UO_6: 40.8(5)	MnO: 11.4(2)	
$SrFe_{0.128(6)}U_{0.872(6)}O_3$: 42.4(8)	$SrUO_{3.948}$: 1.42(3)	Sr_3UO_6: 20.4(5)	Fe^0: 35.8(5)
$SrCo_{0.212(4)}U_{0.788(4)}O_3$: 62.2(1)	$SrUO_{3.948}$: 5.90(7)	Sr_3UO_6: 28.3(6)	Co^0: 3.64(14)
$SrNi_{0.206(4)}U_{0.794(4)}O_3$: 69.4(9)	$SrUO_{3.948}$: 6.8(1)	Sr_3UO_6: 20.6(5)	Ni^0: 3.2(1)
$SrZn_{0.236(4)}U_{0.764(4)}O_3$: 75(1)	$SrUO_{3.948}$: 3.09(4)	Sr_3UO_6: 22.4(5)	[a]

[a] Segregated ZnO sublimates during the reduction process.

state of U is 4.62+. Fig. 7 shows the thermal evolution of the magnetic susceptibility of the Zn reduced perovskite, showing a paramagnetic behavior at high temperatures; a fit to the Curie–Weiss law in the paramagnetic region (inset of Fig. 7) yields a linear regression with a Curie molar constant $C = 0.872$ emu K/mol Oe, μeff = 2.64 μB and a Weiss constant $\theta = -325.62$ K indicating predominant AFM interactions. The theoretical values of the paramagnetic moment for U^{5+} and U^{4+} are 2.54 and 3.58 μB/atom respectively. For the $SrZn_{0.236(4)}U_{0.764(4)}O_3$ stoichiometry the expected magnetic moment for U^{5+} or U^{4+} would be 2.22 or 3.13 μB/f.u.; the observed paramagnetic moment (2.64 μB) corresponds to a intermediate U^{5+}/U^{4+} oxidation state, as estimated from the nominal stoichiometry. The inset of Fig. 7 seems to indicate an antiferromagnetic ordering below 30 K,

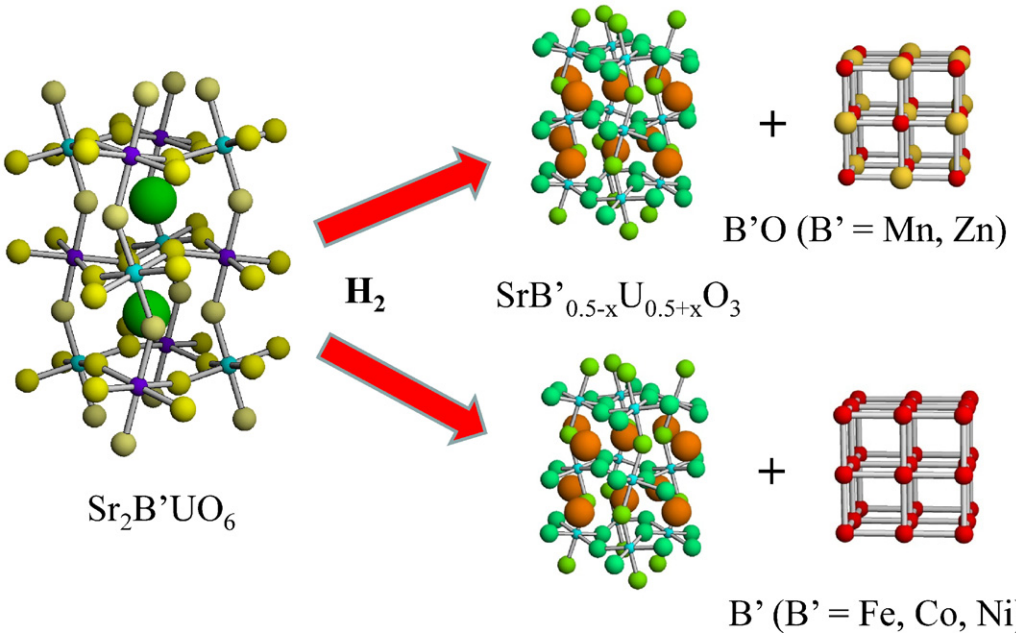

Fig. 6. The two reduction mechanisms of the $Sr_2B'UO_6$ double perovskites via segregation of metal (B′ = Fe, Co, Ni) or to B′O (B′ = Mn, Zn).

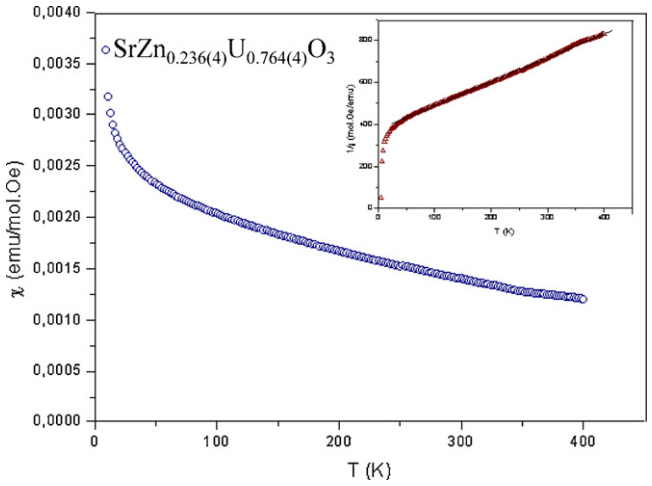

Fig. 7. Thermal variation of the magnetic susceptibility for $SrZn_{0.236(4)}U_{0.764(4)}O_3$. Inset: inverse of the magnetic susceptibility.

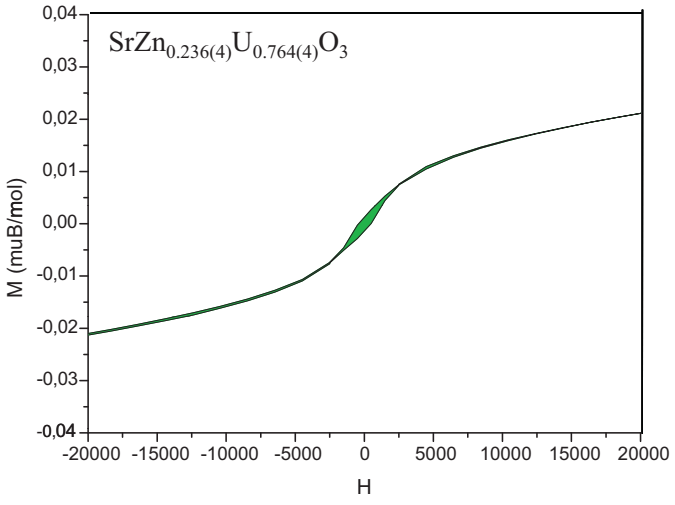

Fig. 8. Magnetization vs. magnetic field isotherm (T = 5 K) for $SrZn_{0.236(4)}U_{0.764(4)}O_3$.

manifested as a sudden deviation from the linear behavior and supported by the highly negative θ_W value. The magnetization versus magnetic field curve at 5 K Fig. 8 exhibits a small hysteresis cycle and small saturation magnetization of 0.02 μB/f.u. that strongly suggests the presence of weak ferromagnetic local interactions or a canted antiferromagnet. Due to the character of this simple, disordered $SrZn_{0.236(4)}U_{0.764(4)}O_3$ perovskite, where magnetic U cations and non-magnetic Zn^{2+} cations are distributed at random over the octahedral positions, the magnetic behavior can be explained by the AFM coupling of pairs of U^{5+}/U^{4+} magnetic moments in naturally-occurring U-rich regions of the crystal structure.

5. Conclusions

The reduction of the long-range ordered double perovskites $Sr_2B'UO_6$ leads to simple perovskites of composition $SrB'_{0.5-x}U_{0.5+x}O_3$, with segregation of B′ metal or B′O (depending on the formation Gibbs energies of the monoxides) and the concomitant reduction of U from hexavalent to pentavalent/tetravalent. This structural evolution has been confirmed by Rietveld analysis from XRPD data of the reduced phases. The full antisite B′/U disordering observed in the Pnma, reduced perovskites with respect to the long-range ordering observed on the oxidized $Sr_2B'UO_6$ double perovskites is due to the decrease of the charge difference of both B′ and U cations. The magnetic behavior of the Zn-containing compound, where the magnetic response comes exclusively from reduced U ions, confirms the U^{5+}/U^{4+} oxidation state of the actinide element and suggests a magnetic behavior arising from the strong AFM coupling between U^{5+}/U^{4+} neighbors, yielding an uncompensated antiferromagnet with a small saturation magnetization.

Acknowledgements

J.C.P., M.C.V. and R.M.P. thank CONICET (Project PIP No. 01360/08), SECYT-UNSL (Project 7707) and ANPCYT (Project PICT 25459). J.C.P. and R.E.C. are members of CONICET. R.E.C. thanks ANPCYT (PICT2007 00303), CONICET and SECYT-UNC for financial support. J.A.A. and M.J.M.L. thank the financial support of the Spanish Ministry of Science and Innovation to the project MAT2010-16404.

References

[1] M.T. Anderson, K.B. Greenwood, G.A. Taylor, K.R. Poeppelmeier, Prog. Solid State Chem. 22 (1993) 197.
[2] W. Sleight, J.L. Gillson, P.E. Bierstedt, Solid State Commun. 17 (1975) 27.
[3] D.E. Cox, A.W. Sleight, R.M. Moon (Eds.), Proceedings of the Conference on Neutron Scattering, National Technical Information ServiceSpringfield, VA, Gatlinburg, (1976), p. 45.
[4] M.A. Akbas, P.K.J. Davies, Am. Ceram. Soc. 81 (1998) 670.
[5] I.M. Reaney, E.L. Colla, N. Setter, Jpn. J. Appl. Phys. 33 (1994) 3984.
[6] K.-I. Kobayashi, T. Kimura, H. Sawada, K. Terakura, Y. Tokura, Nature (London) 395 (1998) 677.
[7] A. Maignan, B. Raveau, C. Martin, M. Hervieu, J. Solid State Chem. 144 (1999) 224.
[8] T.H. Kim, M. Uehara, S.W. Cheong, S. Lee, Appl. Phys. Lett. 74 (1999) 1737.
[9] M.C. Viola, M.J. Martinez-Lope, J.A. Alonso, P. Velasco, J.L. Martinez, J.C. Pedregosa, R.E. Carbonio, M.T. Fernandez-Diaz, Chem. Mater. 14 (2002) 812.
[10] D.P. Fagg, V.V. Kharton, A.V. Kovalevsky, A.P. Viskup, E.N. Naumovich, J.R. Frade, J. Eur. Ceram. Soc. 21 (2001) 1831.
[11] R.M. Pinacca, M.C. Viola, J.C. Pedregosa, M.J. Martínez-Lope, R.E. Carbonio, J.A. Alonso, J. Solid State Chem. 180 (2007) 1582.
[12] R.M. Pinacca, M.C. Viola, J.C. Pedregosa, A. Muñoz, J.A. Alonso, R.E. Carbonio, J. Dalton Trans. (2005) 447.
[13] H.M. Rietveld, J. Appl. Crystallogr. 2 (1969) 65.
[14] J. Rodríguez-Carvajal, Physica B 192 (1993) 55.
[15] S. Geller, J. Chem. Phys. 24 (1956) 1236.
[16] E.H.P. Cordfunke, D.J.W. IJdo, J. Solid State Chem. 109 (1994) 272.